

1 **Measurement report: Changes in light absorption and molecular**
2 **composition of water-soluble humic-like substances during a winter**
3 **haze bloom-decay process in Guangzhou, China**

4
5 Chunlin Zou^{1,3}, Tao Cao^{1,3}, Meiju Li^{1,3}, Jianzhong Song^{1,2,4,*}, Bin Jiang^{1,2}, Wanglu Jia^{1,2},
6 Jun Li^{1,2}, Xiang Ding^{1,2}, Zhiqiang Yu^{1,2,4}, Gan Zhang^{1,2}, Ping'an Peng^{1,2,3,4}

7 ¹State Key Laboratory of Organic Geochemistry and Guangdong Provincial Key
8 Laboratory of Environmental Protection and Resources Utilization, Guangzhou Institute
9 of Geochemistry, Chinese Academy of Sciences, Guangzhou 510640, China

10 ²CAS Center for Excellence in Deep Earth Science, Guangzhou 510640, China

11 ³University of Chinese Academy of Sciences, Beijing 100049, China

12 ⁴Guangdong-Hong Kong-Macao Joint Laboratory for Environmental Pollution and
13 Control, Guangzhou 510640, China

14

15 **Correspondence to: Jianzhong Song (songjzh@gig.ac.cn)*

16

17

18 **Abstract**

19 Water-soluble humic-like substances (HULIS) absorb light in near-UV and visible
20 wavelengths and exert significant influence on the atmospheric environment and climate.
21 However, knowledge on HULIS evolution during haze bloom-decay process is limited.
22 Herein, PM_{2.5} samples were obtained during a winter haze event in Guangzhou, China,
23 and light absorption and molecular composition of HULIS were investigated by UV-vis
24 spectrophotometry and ultrahigh-resolution mass spectrometry. Compared with HULIS
25 in clean days, the absorption coefficients (Abs_{365}) of HULIS in haze days were
26 significantly higher but the mass absorption efficiencies (MAE_{365}) were relatively lower,
27 suggesting diverse and dynamic absorption properties of HULIS during haze episodes.
28 The CHO and CHON compounds were the most abundant components in HULIS,
29 followed by CHOS, CHONS, and CHN. Haze HULIS presented comparatively higher
30 molecular weight, lower aromaticity index (AI_{mod}), and higher O/C_w , O/N_w , and O/S_w
31 ratios, indicating that HULIS fractions undergo relatively higher oxidation during haze
32 days than clean days. Moreover, CHON and CHO compounds with high AI_{mod} were the
33 major potential chromophores in HULIS and significantly contributed to HULIS light
34 absorption. It's worth noting that the proportions of these chromophores were decreased
35 during haze event, mainly owing to their higher oxidation during haze episode. Besides,
36 accumulated contribution of organic compounds emitted from vehicles and formed from
37 reactions of bio-VOCs also diluted light-absorbing compounds in haze HULIS. These
38 findings help to understand HULIS evolution during haze bloom-decay process in the
39 subtropic region of China.

40

41 **1. Introduction**

42 Water-soluble humic-like substances (HULIS), belonging to a class of highly
43 complex organic compounds with physical/chemical properties similar to humic
44 substances in natural aquatic/soil environments, which constitute 30%–70% of water-
45 soluble organic compounds in ambient aerosols and are responsible for > 70% of light
46 absorption (at 365 nm) in water-soluble brown carbon (BrC) (Graber and Rudich, 2006;
47 Laskin et al., 2015; Huang et al., 2018). They are thought to be comprised of aromatic
48 structures containing aliphatic side chains and oxygenated functional groups such as
49 hydroxyl, carboxyl, nitrate, and organosulfate groups (Lin et al., 2012; Song et al., 2018;
50 Zeng et al., 2020). HULIS are ubiquitously identified in atmospheric aerosols, fog, cloud,
51 and rain water, and have been demonstrated to play significant effects on both
52 atmospheric environment and climate (Bianco et al., 2018; Wu et al., 2018; Zhan et al.,
53 2022). In addition, HULIS exert adverse health effects because they can enhance the
54 oxidative potential of organic aerosols (Ma et al., 2019; Cao et al., 2021).

55 In recent years, severe particulate pollution (i.e., haze events) frequently occur in
56 some developing country such as China, which has drawn extensive public and scientific
57 concerns (An et al., 2019; Zhang et al., 2020). According to An et al. (2019),
58 contributions of organic aerosols, including primary organic aerosols and secondary
59 organic aerosols (SOA), are significant for severe haze events; in particular, the
60 contribution of SOA in China is expected to continuously increase because of stronger
61 chemical reactions in the atmosphere. HULIS are an important component in organic
62 aerosols, which originate from a variety of primary emissions (e.g., biomass burning
63 (BB), coal combustion, off-road engine emission) (Fan et al., 2016; Cui et al., 2019; Tang

64 et al., 2020) and secondary chemical oxidation of biogenic and anthropogenic volatile
65 organic compounds (VOCs) (Yu et al., 2016; Tomaz et al., 2018) and soot (Fan et al.,
66 2020). During the haze episode, a number of chemical processes occur in aqueous phase
67 (Wong et al., 2017; Wu et al., 2018) and gas phase (Sumlin et al., 2017), which lead to
68 significant changes in chemical composition and light absorption properties of HULIS.
69 For instance, recent studies on oxidation of BB-derived BrC have indicated that although
70 both enhancement and bleaching of BrC occur during aging, bleaching of BrC becomes
71 dominant over a long period (Fan et al., 2020; Wong et al., 2017; Ni et al., 2021).
72 However, multiphase reaction between carbonyl and amine has demonstrated rapid
73 formation of light-absorbing organic compounds (Kampf et al., 2016). Nevertheless, it
74 should be noted that these results were mainly obtained from laboratory experiments and
75 may not reflect the complex evolution behavior of BrC in atmospheric environment.

76 High concentrations of HULIS have been determined during typical haze episodes
77 in northern, eastern, and southern China (Fan et al., 2016; Zhang et al., 2020; Wang et al.,
78 2020), and have been demonstrated to significantly influence atmospheric visibility,
79 environment, and photochemical process. Guangzhou is the biggest city in the Pearl
80 River Delta (PRD), one of the most developed regions in China, and is located in the
81 subtropical zone with a population of over 18 million people (Yu et al., 2017). Although
82 a remarkable decline in atmospheric particulate matter (PM_{2.5}) pollution has been
83 observed in recent years owing to strict regulatory controls, O₃ and VOCs still remain at
84 higher levels and severe haze pollution caused by fine particulate matter frequently occur
85 in winter (An et al., 2019; Li et al., 2019; Yang et al., 2022). Several studies have
86 investigated the optical, chemical, and molecular properties of HULIS in the PRD region

87 (Lin et al., 2010, 2012; Fan et al., 2016; Liu et al., 2018; Jiang et al., 2020, 2021). For
88 example, the studies on the temporal variations of water-soluble HULIS in Guangzhou
89 indicated that HULIS had higher concentrations and mass absorption efficiencies
90 (MAE_{365}) in the winter, which were attributed to the increasing contribution of BB and
91 secondary nitrate formation in the winter monsoon period (Fan et al., 2016; Jiang et al.,
92 2020, 2021). In addition, the molecular composition of HULIS (and BrC) in the PRD
93 region were also investigated and demonstrated that the levels of unsaturated and
94 aromatic structures are the important factor influencing their light absorption properties
95 (Jiang et al., 2020). However, detailed information regarding the evolution of light
96 absorption and molecular composition of HULIS during haze events is still scarce.

97 Recently, ultrahigh-resolution Fourier transform ion cyclotron resonance mass
98 spectrometry (FT-ICR MS) coupled with electrospray ionization (ESI) sources has been
99 frequently employed to investigate the molecular characteristics of HULIS in ambient
100 aerosols (Song et al., 2018, 2022; Tang et al., 2020; Zeng et al., 2021). Owing to its
101 extremely high mass resolution and accuracy, this technique allows further exploration of
102 the evolution of HULIS during haze event. The present study performed comprehensive
103 characterization of HULIS in $PM_{2.5}$ collected during a haze event in Guangzhou, China.
104 The abundances and light absorption properties of HULIS were first measured, and
105 carbonaceous fractions, water-soluble ions, and levoglucosan (Lev) were determined.
106 Subsequently, four HULIS samples collected during different haze stages were analyzed
107 using FT-ICR MS operated in both ESI⁻ and ESI⁺ modes. To the best of our knowledge,
108 the present study is the first to apply a combination of optical properties and molecular
109 characterization by FT-ICR MS to investigate HULIS in a haze event in the subtropical

110 zone of China. The results obtained provide novel insights into the evolution of HULIS
111 during haze event, and are important for predicting the environmental and climatic effects
112 of HULIS in South China.

113 **2. Material and Methods**

114 **2.1. Aerosol sampling**

115 The PM_{2.5} samples were collected on the campus of Guangzhou Institute of
116 Geochemistry, Chinese Academy of Sciences, Guangzhou, China (23.14N, 113.35E),
117 which is an academic and residential region. Traffic emissions and residential activities
118 are the potential pollution sources in the sampling area. The 24-h PM_{2.5} sampling was
119 conducted using a high-volume sampler (Tianhong Intelligent Instrument Plant, Wuhan,
120 China, with a flow rate of 1.0 m³ min⁻¹) during 7 to 30 January of 2018, and a total of 24
121 samples were collected on the prebaked quartz filters (20.3 × 25.4 cm², Whatman,
122 Maidstone, UK). Field blank samples were collected by keeping a blank filter in the
123 sampler without pumping air. Before sampling, the filters were wrapped in aluminum foil
124 and prebaked at 450°C for 6 h to remove carbonaceous impurities. Before and after
125 sampling, the filters were weighed at 25°C and 50% RH on a microbalance (Sartorius
126 Model BP210D). The PM_{2.5} concentrations were determined by weighing the filters
127 before and after collection. Finally, all filter samples were stored in a refrigerator at -20 °C
128 until analysis. The mass accuracy achieved was < 2% based on triplicate analyses of filter
129 samples. Meteorological data (<http://www.wunderground.com/history/airport/ZGGG>),
130 including wind speed, temperature, relative humidity, and concentrations of SO₂, O₃, and
131 NO₂, for the sampling days are presented in Figure 1 and Table S1.

132 **2.2. Isolation of HULIS**

133 HULIS were isolated using a water extraction and solid-phase extraction (SPE)
134 procedure as described previously (Zou et al., 2020). This method has been used in most
135 previous studies because of its easy operation and high reliability and reproducibility and
136 low limit of detection (Fan et al., 2002), therefore, it was also used in this study. Briefly,
137 portions of the PM_{2.5} samples (100 cm²) were ultrasonically extracted with 50 mL of
138 ultrapure water for 30 min. The extracts were filtered through a 0.22- μ m PTFE syringe
139 filter to remove the suspended insoluble particles. About 50 mL of water extracts were
140 obtained from each sample, of which 20 mL was used for the isolation and analysis of
141 HULIS, 20 mL for analysis of water-soluble organic carbon (WSOC), and the remained
142 extracts for the analysis of inorganic ions, respectively. Then, the 20 mL water extracts
143 were adjusted to pH of 2 with HCl, and loaded on a preconditioned SPE cartridge (Oasis
144 HLB, 200 mg/6 mL, Waters, USA). The hydrophilic fraction (i.e., inorganic ions, high-
145 polar organic acids, etc) was removed with ultrapure water, whereas the relatively
146 hydrophobic HULIS fraction was retained and eluted with 2% (v/v) ammonia/methanol.
147 Finally, HULIS solution was evaporated to dryness with a gentle N₂ stream and
148 redissolved with ultrapure water for the analysis.

149 It is noted that the HULIS here is the hydrophobic portion of water-soluble organic
150 matter, which can be isolated with different types of SPE columns (e.g., HLB, C-18,
151 DEAE, XAD-8, and PPL) (Fan et al., 2012, 2013; Lin et al., 2012; Zou et al., 2020; Jiang
152 et al., 2020). Although each resin type has its special chemical properties, the
153 hydrophobic HULIS isolated with different sorbents were similar in chemical, molecular
154 properties based on previous studies (Fan et al., 2012, 2013; Zou et al., 2020). Therefore,

155 for better comparison with other studies, the hydrophobic fractions isolated by SPE
156 methods were all termed as HULIS in the present paper.

157 **2.3. Light absorption analysis**

158 The absorption spectra of the WSOC and HULIS fractions were measured by a UV-
159 vis spectrophotometer (UV-2600, Shimadzu) between 200 to 700 nm. Each spectrum was
160 corrected for the filter blanks. The light absorption coefficients, absorption Ångström
161 exponent (AAE) and mass absorption efficiency (MAE_{λ}) were calculated and the detailed
162 methods are presented in the Supporting Information (SI).

163 **2.4. Chemical analysis**

164 For FT-ICR MS analysis, the HULIS samples were isolated from $PM_{2.5}$ collected
165 during four periods: before haze days (clean-I days, 7–12 January), haze bloom days
166 (haze-I days, 13–18 January), haze decay days (haze-II days, 19–24 January), and after
167 haze days (clean-II days, 25–30 January). A filter punch (18 cm in diameter) was taken
168 from every sample, and all the six samples in each period was combined for the isolation
169 of HULIS fractions. The obtained HULIS samples were measured with an ESI FT-ICR
170 MS (Bruker Daltonik GmbH, Bremen, Germany) equipped with a 9.4 T refrigerated
171 actively shielded superconducting magnet. The system was operated in both ESI⁻ and
172 ESI⁺ modes. The scan range was set to m/z from 100 to 1000, with a typical mass-
173 resolving power >450,000 at m/z 319 with <0.2 ppm absolute mass error. The mass
174 spectra were calibrated externally with arginine clusters and internally recalibrated with
175 typical O_5 -class species peaks in DataAnalysis 4.4 (Bruker Daltonics). Due to the
176 inherent differences in the ionization mechanisms between ESI⁻ and ESI⁺ modes, the

177 data detected by the two ionization modes can provide complementary information on the
178 molecular composition of atmospheric HULIS (Lin et al., 2012; Lin et al., 2018). The
179 details of data analysis are provided in the SI.

180 The amounts of organic carbon (OC) and elemental carbon (EC) were determined by
181 a OC/EC analyzer (Sunset Laboratory Inc., USA) (Mo et al., 2018). The concentrations
182 of WSOC and HULIS were determined by a TOC analyzer (Shimadzu TOC_VCPH,
183 Kyoto, Japan). The water-soluble inorganic species (NO_3^- , SO_4^{2-} , Cl^- , NH_4^+ , K^+ , Na^+ ,
184 Ca^{2+} , Mg^{2+} ,) were measured with a Dionex ICS-900 ion chromatography system (Thermo
185 Fisher Scientific, USA) as described previously (Huang et al., 2018). The concentrations
186 of Lev were analyzed with a gas chromatography–MS after derivatization with BSTFA
187 and pyridine at 70 °C for 3 h (Huang et al., 2018). Detailed information regarding these
188 measurements is provided in the SI.

189 **3. Results and Discussion**

190 **3.1. Abundance and chemical composition of PM_{2.5}**

191 Figure 1 shows the meteorological conditions, PM_{2.5} concentration, and
192 concentrations of major chemical constituents, including carbon fractions and water-
193 soluble inorganic ions in PM_{2.5} samples obtained during a haze bloom-decay process.
194 Based on the variation in PM_{2.5} concentration, these samples were categorized into four
195 groups: clean-I days (before haze, 14–24 $\mu\text{g m}^{-3}$), haze-I days (haze bloom, 45–114 μg
196 m^{-3}), haze-II days (haze decay, 58–115 $\mu\text{g m}^{-3}$), and clean-II days (after haze, 9–35 μg
197 m^{-3}). As indicated in Table S1 and Figure 1, the PM_{2.5} concentrations increased from 18
198 $\pm 3.3 \mu\text{g m}^{-3}$ in clean-I days to 82 ± 26 and $84 \pm 22 \mu\text{g m}^{-3}$ in haze-I and haze-II days,

199 respectively, and then decreased to $21 \pm 10 \mu\text{g m}^{-3}$ in clean-II days. This finding
200 obviously indicated that the average $\text{PM}_{2.5}$ concentrations during the examined haze
201 episode are higher than the second-grade national ambient air quality standard in China
202 ($75 \mu\text{g m}^{-3}$, 24 h), whereas those during clean days are lower than the first-grade national
203 ambient air quality standard in China ($35 \mu\text{g m}^{-3}$, 24 h). However, the average $\text{PM}_{2.5}$
204 concentrations during the haze event are lower than those in the cities in winter haze,
205 including Shenyang ($108 \mu\text{g m}^{-3}$) (Zhang et al., 2020), and Nanjing ($123 \pm 28.5 \mu\text{g m}^{-3}$)
206 (Li et al., 2020), Beijing ($158 \mu\text{g m}^{-3}$) and Xi'an ($345 \mu\text{g m}^{-3}$) (Zhang et al., 2018).

207 As shown in Table S1, the average concentrations of OC and EC were 2.2–15 and
208 $0.36\text{--}2.7 \mu\text{gC m}^{-3}$ in the four stages, respectively, implying that the distinct changes in
209 OC and EC were higher during haze episodes than those in clear days. During the entire
210 study period, WSOC concentration ranged from 0.5 to $12.5 \mu\text{gC m}^{-3}$ ($4.3 \pm 1.2 \mu\text{gC m}^{-3}$),
211 which contributed to 53%–57% of OC in $\text{PM}_{2.5}$. The HULIS concentration noted in the
212 present study ranged from 0.15 to $6.1 \mu\text{gC m}^{-3}$ ($2.2 \pm 1.9 \mu\text{gC m}^{-3}$), which was
213 comparable to those observed in the PRD region, such as Hong Kong ($2.38 \pm 1.62 \mu\text{gC}$
214 m^{-3}) (Ma et al., 2019), Guangzhou ($2.4 \pm 1.6 \mu\text{gC m}^{-3}$) (Fan et al., 2016), and Heshan
215 ($2.08 \pm 1.16 \mu\text{gC m}^{-3}$) (Jiang et al., 2020), but lower than those in northern cities of
216 China, such as Xi'an ($12.4 \pm 6.5 \mu\text{gC m}^{-3}$) (Huang et al., 2020), Beijing (3.79 ± 3.03
217 $\mu\text{gC m}^{-3}$) (Mo et al., 2018), and Lanzhou ($4.7 \mu\text{gC m}^{-3}$) (Tan et al., 2016). As shown in
218 Figure 1, HULIS also exhibited obvious variations during the entire sampling period. The
219 average HULIS concentration was $0.46 \pm 0.22 \mu\text{gC m}^{-3}$ in clean-I days, which sharply
220 increased to $4.5 \pm 1.2 \mu\text{gC m}^{-3}$ in haze-I days, then decreased to $3.1 \pm 1.2 \mu\text{gC m}^{-3}$ in
221 haze-II days, and rapidly declined to $0.75 \pm 0.52 \mu\text{gC m}^{-3}$ in clean-II days. This result

222 was consistent with the changing trend of WSOC, OC, and EC. In addition, the
223 HULIS/WSOC ratios were about 0.50 ± 0.13 in the $PM_{2.5}$ samples, which are in broad
224 agreement with other studies showing that HULIS is the major fraction of WSOC (Fan et
225 al., 2016; Ma et al., 2019; Jiang et al., 2020).

226 As illustrated in Figure 1, obvious variations in chemical compositions were also
227 observed in these $PM_{2.5}$ samples. Secondary inorganic aerosols (SIA) (i.e., SO_4^{2-} , NO_3^- ,
228 and NH_4^+), OC, and EC exhibited a similar variation during the entire study period, and
229 their contents sharply increased from 10 January in clean-I days to 13–18 January in
230 haze-I days, then slowly decreased in haze-II days, and finally reached lower levels in
231 clean-II days. It must be noted that the increasing rate of EC was similar to that of SIA in
232 haze-I days, indicating that direct emissions and atmospheric reactions may play similar
233 roles in $PM_{2.5}$ increase during this haze bloom period. As indicated in Figure 1f, the
234 highest values of NO_3^-/SO_4^{2-} were observed in haze-I days, implying the important
235 influence of traffic exhausts in the haze bloom period (Mo et al., 2018). In addition, the
236 high NO_2 and O_3 concentrations and the stable meteorological condition with high
237 temperature also led to the outburst of fine particulate pollution in this period. During
238 haze-II days, the SIA and OM contents in $PM_{2.5}$ slowly decreased, whereas the
239 concentrations of Na^+ , Cl^- , and unidentified materials in $PM_{2.5}$ increased (Figure 1e,h),
240 suggesting that local contribution weakened and regional contribution via sea salt became
241 more important (Jiang et al., 2021). This phenomenon was also observed to be consistent
242 with the changes in the pollutant sources transported by air masses. As indicated in
243 Figure S1, the $PM_{2.5}$ samples in haze-II days included some contributors transported from

244 coastal area of eastern Guangdong Province and Fujian Province, and the $PM_{2.5}$ are likely
245 to be enriched with sea salt materials and mineral dusts.

246 **3.2. Light absorption**

247 The light absorption properties of WSOC and HULIS (Figure 1d, i, j and Table S2)
248 exhibited obvious temporal variations during the sampling period. The AAE values of
249 WSOC and HULIS ranged from 4.1 to 6.4 and 5.6 to 6.6, respectively. The AAE values
250 for HULIS were obviously higher than those for WSOC in the same sample (Figure 1i),
251 indicating that light absorption of HULIS is more wavelength-dependent than that of
252 WSOC. Similar results were also observed in previous studies (Park et al., 2018; Jiang et
253 al., 2020; Cao et al., 2021). These differences could be attributed to the differences in
254 chemical composition of chromophores in WSOC and HULIS. As shown in Table S2, the
255 E_{250}/E_{365} values of HULIS (5.3–5.6) all higher than that (4.4–5.1) of WSOC, suggested
256 that the light-absorbing species in HULIS may have relative lower aromaticity and/or
257 lower molecular weight than those in WSOC (Chen et al., 2016; Li and Hur, 2017).
258 Therefore, the HULIS fractions exhibit relative higher absorption at UV and short visible
259 wavelengths and relative lower absorption at long visible wavelengths, which resulting in
260 relative higher AAE values. Moreover, the AAE values of HULIS did not present
261 significant variation during the entire haze process, which could be related with the
262 evolution of HULIS chromophores in different stages (Jiang et al., 2020; Huang et al.,
263 2018; Deng et al., 2022). At first, the enhanced oxidation of aromatic species in haze
264 days could lead to the bleaching or degradation of chromophores (a detailed explanation
265 was provided in Section 3.3), thus a less wavelength dependence (Forrister et al., 2015;
266 Zhan et al., 2022). In contrast, the outburst of secondary organic aerosols and the

267 photolysis of organic aerosols in haze days both tended to the higher AAE values (Saleh
268 et al., 2013; Dasari et al., 2019). Consequently, the different trends in AAE were
269 counterbalanced during the haze days, which resulting in no significant AAE variations
270 were observed for HULIS in entire sampling process. This is also consistent with the
271 trends of the E_{250}/E_{365} ratios of HULIS in the four stages (Table S2).

272 Light absorption at 365 nm (Abs_{365}) for WSOC and HULIS were 2.5 ± 2.0 and $1.8 \pm$
273 1.6 M m^{-1} , respectively (Table S2). HULIS contributed to about 72% of light absorption
274 coefficients by WSOC, implying that they enriched the major light-absorbing
275 components in WSOC. As shown in Figure 1d, the Abs_{365} values for HULIS presented
276 obvious temporal variations. The $Abs_{365,HULIS}$ value was $0.55 \pm 0.06 \text{ M m}^{-1}$ in clean-I
277 days, which first increased to $3.4 \pm 1.5 \text{ M m}^{-1}$ in haze-I days and then slowly decreased to
278 $2.6 \pm 0.85 \text{ M m}^{-1}$ in haze-II days, and finally rapidly declined to $0.64 \pm 0.32 \text{ M m}^{-1}$ in
279 clean-II days. This result was similar to the variations in the mass concentration of
280 HULIS. Furthermore, the Abs_{365} values for HULIS in Guangzhou were found to be
281 higher than those observed in southeastern Tibetan Plateau ($0.38\text{--}1.0 \text{ M m}^{-1}$) (Zhu et al.,
282 2018), but obviously lower than those in Xi'an ($7.6\text{--}36 \text{ M m}^{-1}$) (Shen et al., 2017) and
283 Beijing, ($3.7\text{--}10.1 \text{ M m}^{-1}$) (Du et al., 2014).

284 In general, MAE_{365} value can be used to assess the light absorption capacity of target
285 organic compounds (Li et al., 2019). As shown in Figure 1j and Table S2, the average
286 MAE_{365} value for WSOC was $1.0 \pm 0.21 \text{ m}^2 \text{ gC}^{-1}$ ($0.68\text{--}1.3 \text{ m}^2 \text{ gC}^{-1}$), nearly same to
287 $1.1 \pm 0.27 \text{ m}^2 \text{ gC}^{-1}$ ($0.77\text{--}1.8 \text{ m}^2 \text{ gC}^{-1}$) for HULIS, during the entire sampling period.
288 Moreover, the MAE_{365} values for HULIS measured in the present study were noted to be
289 dropped in the ranges of those determined in Beijing ($1.43 \pm 0.33 \text{ m}^2 \text{ g C}^{-1}$) (Mo et al.,

290 2018), Xi'an ($0.91\text{--}1.85\text{m}^2 \text{ g C}^{-1}$) (Yuan et al., 2021), and Hong Kong ($1.84 \pm 0.77 \text{ m}^2$
291 gC^{-1}) (Ma et al., 2019). The average MAE_{365} values for HULIS exhibited some temporal
292 variations. The MAE_{365} values for HULIS were 0.91 ± 0.03 and $0.95 \pm 0.11 \text{ m}^2 \text{ gC}^{-1}$ in
293 haze-I and haze-II days, respectively, which were lower than those (1.3 ± 0.22 and $1.3 \pm$
294 $0.27 \text{ m}^2 \text{ gC}^{-1}$, respectively) observed in clean-I and clean-II days, suggesting that HULIS
295 have a relatively weaker light absorption capability in haze days. This finding is
296 consistent with the results reported by Zhang et al. (2017), who found that the MAE_{365}
297 values in the heating or non-heating seasons during hazy days were lower than those in
298 clean days. These differences in MAE_{365} values may potentially contribute to the
299 enhanced oxidation reaction that was derived by the increased O_3 levels and high
300 temperature and relative humidity (RH) during haze days (Figure 1). This oxidation
301 process would lead the chromophores containing C=C unsaturated bond to be severely
302 degraded (Wang et al., 2017a; Zhang et al., 2017). Besides, an increase in additional
303 sources for HULIS in the study area, such as weaker or non-light-absorbing compounds
304 formed by atmospheric oxidation, could also result in weaker light absorption of HULIS
305 during the haze episode (Liu et al., 2018).

306 **3.3. Molecular evolution of HULIS during the haze process**

307 For an in-depth understanding of the variation in HULIS at molecular level during
308 the haze process, the four HULIS samples collected in different stages of the haze
309 process were analyzed by ESI FT-ICR MS in both negative and positive modes. As
310 shown in Figure 2, thousands of peaks were detected in the mass range between m/z 100
311 and m/z 700, with the high intensity ions noted within m/z 150–400. It is obvious that
312 some organic compounds with stronger arbitrary abundance were labeled, and their

313 formulas, double bond equivalent (DBE), modified aromaticity index (AI_{mod}), and
314 potential sources were listed in Table S3. Compounds a ($C_7H_7NO_3$) and b ($C_8H_6O_4$), both
315 have high DBE values, which might be assigned to aromatics such as methylnitrophenol
316 and phthalic acid, whereas compound d ($C_8H_{18}O_4S$) with low DBE value and high O/S
317 ratio was probably aliphatic organosulfate. According to previous studies, these organic
318 molecules might be derived from BB and diesel fuel and thereby these results suggested
319 that both BB and vehicular emissions are important sources of BrC in ambient aerosols
320 (Mohr et al., 2013; Riva et al., 2015; Blair et al., 2017). Furthermore, compound e
321 ($C_{10}H_{17}NO_7S$) and compound f ($C_{10}H_{18}N_2O_{11}S$) in Table S3 were found to be identical to
322 the oxidation products of monoterpenes, suggest that biogenic sources could contribute to
323 the formation of HULIS (Surratt et al., 2008; Wang et al., 2019). Thus, HULIS could be
324 affected by multiple sources during the haze process, possibly including BB, biogenic
325 sources, and anthropogenic emissions.

326 The identified formulas could be divided into seven compound categories, namely,
327 CHO^- , $CHON^-$, $CHOS^-$, and $CHONS^-$ detected in ESI^- mode and CHO^+ , CHN^+ , and
328 $CHON^+$ detected in ESI^+ mode. As illustrated in Figure 2, the CHO compounds were the
329 most abundant group in all the HULIS, accounting for 43%–50% and 51%–57% of the
330 overall compounds detected in the ESI^- and ESI^+ modes, respectively. It must be noted
331 that relatively lower contents of CHO^- were detected during the haze episode (haze-I and
332 haze-II days) and CHO^+ molecules in haze-I HULIS. The $CHON$ compounds were the
333 second most abundant group in all the HULIS. As shown in Figure 2, the relative content
334 of $CHON^-$ was 23% in clean-I days, which slightly increased to 24%–25% in haze
335 episode, and then decreased to 23% in clean-II days. In contrast, the relative content of

336 CHON⁺ compounds was 41% in clean-I days, which increased to 45% in haze-I days,
337 then fell to 42% in haze-II days and 41% in clean-II days. Both CHOS⁻ and CHONS⁻
338 compounds were identified in all the four HULIS, accounting for 19%–22% and 8%–11%
339 of the total identified compounds, respectively. The CHN⁺ compounds were the least
340 abundant (1.3%–3.6%) in the four HULIS samples, and were relatively higher during the
341 haze episode, especially in haze-I days.

342 Tables S4 and S5 show the relative abundance weighted elemental ratios, molecular
343 weight (MW), DBE, AI_{mod} , and carbon oxidation state (OS_C) for the identified
344 compounds in HULIS. The MW_w values for HULIS determined in the ESI⁻ mode in
345 haze-I and haze-II days were 302 and 283, respectively, which were higher than those in
346 clean-I and clean-II days (266 and 264, respectively). Similar variation was also observed
347 for MW_w for HULIS detected in ESI⁺ mode (Table S5). These results clearly indicated
348 that more higher MW compounds constituted HULIS obtained during the haze episode.
349 Furthermore, the molecular properties of HULIS in different stages of haze process also
350 exhibited some observable differences. As shown in Table S4, the HULIS samples in
351 haze episode detected by ESI⁻ mode presented relatively lower $AI_{mod,w}$ values and
352 relatively higher O/C_w , O/N_w , and O/S_w ratios than those in clean days, indicating that
353 haze HULIS exhibited relatively lower aromaticity and higher oxidation degree than
354 clean HULIS. These differences can be attributed to the enhanced oxidation degradation
355 of aromatic compounds (e.g., phenols, nitroaromatic compounds and polycyclic aromatic
356 hydrocarbons (PAHs)) during the haze process. In addition, increased contribution from
357 traffic emission and secondary reactions of bio-VOCs also decreased the aromaticity and
358 increased the oxidation degree of HULIS (Liu et al., 2016; Tang et al., 2020). These

359 changes in HULIS compounds led to the decrease in their MAE₃₆₅ values during the haze
360 episode, as described above (Zhong and Jang, 2014; Song et al., 2019).

361 **3.3.1. CHO Compounds**

362 The CHO compounds bear O-containing functional groups, and have been
363 frequently detected in ambient aerosols. As shown in Figure 2, the CHO compounds were
364 the predominant component in the four HULIS samples, and the MW_w values for CHO-
365 and CHO+ compounds were 247–288 and 236–272, respectively, with relatively higher
366 MW_w values observed for the CHO group (CHO- and CHO+) in haze HULIS, especially
367 in haze-I samples. This finding may be related to the stronger oxidation of HULIS during
368 haze days, because the aqueous oxidation of biomass burning aerosols was found to yield
369 high MW of organic products (Tomaz et al., 2018; Yu et al., 2016).

370 The OS_C is often used to describe the degree of oxidation of organic species in the
371 atmosphere (Kroll et al., 2011; Wang et al., 2017b). Figure 3 shows plots of OS_C versus
372 carbon number for the CHO compounds. As indicated in the figure, CHO compounds
373 exhibited OS_C from -2 to +1 with up to 40 carbon atoms. Kroll et al. (2011) proposed
374 that compounds with OS_C between -0.5 and +1 and < 18 carbon atoms can be attributed
375 to semi-volatile and low-volatile oxidized organic aerosols (SV-OOA and LV-OOA),
376 which are mainly formed by complex oxidation reactions in atmosphere. Compounds
377 with OS_C between -0.5 and -1.5 and 6–23 carbon atoms are related to primary biomass
378 burning organic aerosol (BBOA). In addition, compounds with OS_C between -1 and -2
379 and ≥18 carbon atoms have been suggested to be hydrocarbon-like organic aerosols
380 (HOA), which are regarded as primary combustion surrogate (Zhang et al., 2005; Kroll et
381 al., 2011; Wang et al., 2017b).

382 As illustrated in Figure 3 and Table S6, most of the CHO⁻ compounds clustered in
383 the BBOA region, accounting for 40%–46% of the total CHO⁻ compounds, thus
384 suggesting that BB may be a major contributor to CHO compounds in HULIS. Figure 3
385 clearly indicates that the majority of aromatic and condensed aromatic compounds
386 produced signals in the OS_C region between -0.5 and 1.0 and carbon number of 3–18
387 (Figure 3), which corresponded to SV-OOA and LV-OOA. The proportions of SV-OOA
388 and LV-OOA accounted for 23%–28% and 1.9%–2.4% of the total CHO⁻ compounds,
389 respectively, and presented no significant variation. In contrast, the HOA components in
390 haze-I days showed the highest abundance (18%), which were much higher than those
391 (3.5%–4.5%) in haze-II, clean-I, and clean-II days. This finding indicated that the
392 increase in the primary source is associated with fossil fuel combustion such as vehicle
393 emissions during the haze bloom period (Zhang et al., 2005).

394 As shown in Figure 3, CHO⁺ compounds presented lower OS_C (from -2.0 to 1.0)
395 than CHO⁻ compounds. Most of the CHO⁺ compounds occurred in the BBOA region in
396 all four HULIS samples, making up to 60%–72% of the total CHO⁺ compounds, which
397 again suggesting that BB is an important contributor to CHO compounds in HULIS. The
398 HOA among CHO⁺ compounds showed the same changing trends as those among CHO⁻
399 compounds, and higher HOA abundance was observed during haze-I days. In addition,
400 some high AI_{mod} values of aromatics were found in the regions A1+ and A2+ (Figure 3),
401 which implied that the highest AI_{mod} values (AI ≥ 0.67) with DBE ≥ 22 were only
402 detected during the haze days possibly owing to soot-derived materials or oxidized PAHs
403 (Decesari et al., 2002; Kuang and Shang, 2020). It must be noted that the sampling site in
404 the present study is influenced by traffic sources, the enhanced oxidation of vehicle-

405 exhausted soot also results in the accumulation of water-soluble high aromatic organic
406 species (Decesari et al., 2002).

407 **3.3.2. CHON Compounds**

408 In the present study, 1379–2217 and 2008–2943 formulas were assigned to CHON
409 compounds identified in the ESI⁻ and ESI⁺ spectra, respectively, which accounted for
410 23%–25% (ESI⁻) and 41%–45% (ESI⁺) of total identified compounds, respectively.
411 Relatively higher contents of CHON⁻ compounds were obviously detected in HULIS
412 samples obtained during haze-I days, suggesting the occurrence of more N-containing
413 components in HULIS during haze bloom days. As shown in Tables S4 and S5, the
414 average MW_w values for CHON⁻ and CHON⁺ compounds were 328 and 317 in haze-I
415 days, respectively, which were slightly higher than those determined in haze-II days and
416 all higher than those observed in clean-I and clean-II days. Meanwhile, the AI_{mod,w} values
417 for CHON⁻ in haze days were 0.31–0.34, which were slightly lower than those in clean
418 days (0.37 and 0.40). These findings indicated that more high MW CHON compounds
419 with lower aromatic structures were formed during the haze episode.

420 The O/N_w ratios for CHON⁻ and CHON⁺ during haze-I and haze-II days were 5.3–
421 5.7 and 3.8, respectively, which were higher than those determined during the two clean
422 periods, confirming that these compounds were highly oxidized during the haze episode
423 (Tables S4 and S5). In general, compounds with O/N ≥ 3 may indicate oxidized N groups
424 such as nitro (–NO₂) or nitrooxy (–ONO₂), whereas compounds with O/N < 3 may denote
425 the reduced N compounds (i.e., amines) (Lin et al., 2012; Song et al., 2018). In the
426 present study, most of the CHON compounds (79%–91% of CHON⁻ compounds and
427 61%–64% of CHON⁺ compounds) exhibited O/N ≥ 3, suggesting that high

428 concentrations of nitro compounds or organonitrates were contained in the CHON
429 compounds. Moreover, these compounds were more abundant in the CHON⁻ group
430 during the haze episode (87%–91%), when compared with those during clean-I and
431 clean-II days (79%–82%), again implying that CHON⁻ compounds undergo relatively
432 higher oxidization during the haze episode. As indicated in Figure 1, the increase in NO₂
433 was consistent with increased production of highly oxidized N-containing organic
434 compounds (NOCs) during the haze episode, which suggested the significant contribution
435 of NO₃-related multigenerational chemistry to organonitrate aerosol formation
436 (Berkemeier et al., 2016).

437 The majority of aromatics and condensed aromatics produced clear signals in
438 regions associated with SV-OOA and LV-OOA (Figure 4). BBOA also constituted a
439 significant proportion (33%–39%) in the CHON⁻ group, and a relatively lower BBOA
440 content was observed in haze-I days. The abundance of HOA was relatively lower,
441 accounting for 2.3%–7.8% of the total CHON compounds, and the relative abundance of
442 HOA in haze-I days was much higher than that in haze-II, clean-I, and clean-II days,
443 suggesting the accumulation of primary fossil fuel combustion during haze-I days.

444 The CHON⁺ compounds mainly occurred at the range of $-2.0 < OS_C < 1.5$, with
445 average OS_C values of around -1.0 for each sample, clearly indicating that CHON⁺
446 compounds were relatively lower than CHON⁻ compounds. Most of the CHON⁺
447 compounds were detected in the BBOA region, accounting for 60%–76% of the total
448 CHON⁺ compounds. The relative contribution of BBOA in haze-I days was lower than
449 that in haze-II and clean days. Moreover, a large number of aromatic species were
450 observed at the region B1⁺ (Figure 4), demonstrating that higher aromatic compounds

451 were only detected in haze-I days, which may be related to soot or BC. Similar trend was
452 also exhibited by CHO+ compounds, indicating the contribution of local combustion
453 sources (e.g., traffic emission) during haze-I days.

454 **3.3.3. CHOS and CHONS Compounds**

455 In this study, 478–696 CHOS compounds and 306–589 CHONS compounds were
456 identified in ESI– mode (Table S4). Among these S-containing compounds, >86% of the
457 CHOS compounds had O/S ratios >4, whereas > 89% of the CHONS compounds
458 presented O/S ratios >7, suggesting that these S-containing compounds were possibly
459 organosulfates and nitrooxyorganosulfates. As listed in Table S4, the $AI_{mod,w}$ values for
460 CHOS and CHONS were about 0.02 and 0.01 in the HULIS fraction, which were much
461 lower than those for CHO and CHON. Almost 99% of the CHOS and CHONS
462 compounds in the HULIS fraction had AI_{mod} values <0.5, while >93% of the CHONS
463 compounds had $AI_{mod} = 0$, indicating that they were mainly comprised of aliphatic and
464 olefinic organosulfates. These results are consistent with the previous findings that the
465 major S-containing compounds among organic aerosols in Guangzhou are organosulfates
466 formed by secondary oxidation reaction of long-chain alkenes/fatty acids with SO_2 (Jiang
467 et al., 2020), which generally possessed long aliphatic carbon chains and a higher degree
468 of oxidation. However, these compounds are different from the S-containing compounds
469 detected during the hazy days in Beijing (Jiang et al., 2016; Mo et al., 2016), which were
470 determined to be aliphatic organosulfates with low degree of oxidation and higher
471 amounts of aromatics and PAH-derived organosulfates, having a strong correlation with
472 anthropogenic emissions.

473 As described earlier, CHOS⁻ and CHONS⁻ compounds might be related to
474 organosulfates or nitrooxyorganosulfates, which have been observed to be derived from
475 atmospheric reactions of bio-VOCs such as α -pinene, limonene, and isoprene (Huang et
476 al., 2018; Surratt *et al.*, 2008) and fossil fuel combustion including coal combustion, off-
477 road engine emissions (Song et al., 2018, 2019; Cui et al., 2019). In the present study, the
478 relative contents of S-containing compounds (CHOS+CHONS) in the HULIS fraction in
479 haze days were all higher than those in clean days (Figure 2). Moreover, the CHOS and
480 CHONS compounds in haze HULIS always have relatively high relatively O/S ratios
481 than those in clean HULIS. These findings suggested the relatively higher contribution of
482 SO₂-related chemical oxidation during the haze event.

483 **3.3.4. CHN Compounds**

484 The N-bases (CHN) are usually identified in ambient aerosols and smokes from BB.
485 In the present study, 110–165 CHN⁺ compounds were identified in ESI⁺ mode, with
486 most of them (>86%) presenting DBE \geq 2, suggesting that they might be nitrile and
487 amine species (Lin et al., 2012). As shown in Figure 2, the abundances of CHN⁺
488 compounds were 2.0%–3.6% in the haze days, which were much higher than those noted
489 in clean days (1.3%–1.4%), indicating higher contribution of CHN⁺ compounds to the
490 HULIS fraction during the haze episode. The MW_w values for CHN⁺ compounds were
491 204–223, which were lower than those for the other groups (i.e., CHO⁺, CHON⁺) (Table
492 S5). However, the average AI_{mod} values for N-bases (0.37–0.48) detected in the ESI⁺
493 mode were much higher than those for CHO⁺ (0.11–0.12) and CHON⁺ (0.20–0.22)
494 compounds, implying that these reduced CHN⁺ compounds exhibited more unsaturated
495 or aromatic structures.

496 To further understand the molecular distribution of CHN⁺ compounds during the
497 haze process, van Krevelen (VK) diagrams were constructed by plotting the H/C ratio
498 versus N/C ratio (Figure S2). It was obvious that this plot could separate the compound
499 classes with different degree of AI. As shown in Figure S2, compounds (denoted in black
500 color) in the upper region of the VK diagram had one N atom with DBE = 0, indicating
501 that they are aliphatic amines. It can be noted from Table S7 that the aliphatic group
502 presented the lowest abundance in all the samples, suggesting that the CHN⁺ compounds
503 possessed comparatively lower aliphatic structures. Olefinic compounds showed the
504 highest abundance in the four samples, which accounted for 37%–51% of the total CHN⁺
505 compounds. Importantly, a large proportion of the compounds (>39%) exhibited high
506 degree of AI (AI > 0.5) (Figure S2 and Table S7), suggesting a large amounts of aromatic
507 structure and N-heterocyclic ring in HULIS. Moreover, the CHN⁺ compounds in haze-I
508 days presented obviously lower content of aromatic structures than those in haze-II,
509 clean-I, and clean-II days, signifying the relatively high contribution of fossil fuel
510 combustion (which generally emits more low-aromatic CHN compounds) during the haze
511 bloom episode(Song et al., 2022). In addition, the CHN⁺ group also constituted a large
512 proportion of BBOA (Table S6), which indicated the significant contribution of BB.
513 However, it must be noted that a relatively lower content of BBOA was detected during
514 haze-I days, which was consistent with the changing trends of CHON⁻ or CHON⁺
515 compounds during the haze episode. These results suggested the relatively lower
516 contribution of BB during haze-I days, because quiet and stable weather conditions can
517 prevent regional transport of BB sources during this stage (Wu et al., 2018).

518 **3.4. Factors influencing light absorption and molecular characteristics of HULIS**
519 **during the haze bloom-decay process**

520 As described earlier, the light absorption properties of HULIS exhibited obvious
521 variation during the haze bloom-decay process. The average Abs_{365} value for HULIS was
522 $0.55 \pm 0.06 \text{ M m}^{-1}$ in clean-I days, which first increased to $3.4 \pm 1.5 \text{ M m}^{-1}$ in haze-I days,
523 then slowly decreased to $2.6 \pm 0.85 \text{ M m}^{-1}$ in haze-II days, and finally rapidly declined to
524 $0.64 \pm 0.32 \text{ M m}^{-1}$ in clean-II days. In general, the light absorption of HULIS can be
525 related to their chemical and molecular properties that are influenced by factors such as
526 sources, secondary formation, and aging process. The results of principal component
527 analysis (PCA) obviously showed a positive loading for principal component 1 (PC1),
528 and the Abs_{365} values for HULIS were clustered with EC, K_{bb}^+ , Lev, NH_4^+ , and NO_3^-
529 (Figure 5). These results suggested that BB and other sources such as new particle
530 formation could contribute to light absorption of HULIS (An et al., 2019; Song et al.,
531 2019). Similarly, the findings of Pearson correlation coefficient analysis revealed that the
532 Abs_{365} values for HULIS exhibited significant positive correlations with K_{bb}^+ ($r = 0.728$,
533 $p < 0.01$) and Lev ($r = 0.800$, $p < 0.01$) (Table S8). As Lev and K_{bb}^+ are generally
534 considered as tracers derived from BB, these results suggested the significant
535 contribution of BB to light absorption of HULIS. This observation was also supported by
536 the abundance of BBOA compounds detected in all the four HULIS samples (Table S6).
537 The significant positive relationships between the Abs_{365} values for HULIS and
538 secondary ions (i.e., NO_3^- ($r = 0.702$, $p < 0.01$), SO_4^{2-} ($r = 0.554$, $p < 0.05$), and NH_4^+ (r
539 $= 0.899$, $p < 0.01$)) indicated the important impact of secondary formation on the light
540 absorption of HULIS. Besides, the Abs_{365} values for HULIS were also strongly correlated

541 with NO₂, O₃, and NO₂, which confirmed the important impact of atmospheric oxidation
542 reactions on the light absorption of HULIS.

543 It must be noted that MAE₃₆₅ is a key parameter signifying the light absorption
544 ability of HULIS. As listed in Table S2, the MAE₃₆₅ values for HULIS varied in different
545 stages, and were lower in haze days owing to the variation in the chemical and molecular
546 composition of HULIS during the haze bloom-decay process. Furthermore, the AI_{mod}
547 values for HULIS varied in different stages (Tables S4), and were relatively lower in
548 haze days, indicating that haze HULIS have comparatively lower degree of conjugation
549 or aromaticity. This finding suggested that the HULIS compounds may undergo higher
550 oxidation during the haze episode, causing a decline in chromophores and reduction in
551 the light absorption capacity of HULIS (Lin et al., 2017). Besides, the accumulated
552 contribution of organic compounds from vehicle emission and secondary chemical
553 reactions of bio-VOCs may also dilute light-absorbing compounds in haze HULIS (Tang
554 et al., 2020; Liu et al., 2016).

555 Lin et al. (2018) reported that potential light-absorbing chromophores can be
556 determined in the region between DBE = 0.5 × C (linear conjugated polyenes C_xH_yC₂)
557 and DBE = 0.9 × C (fullerene-like hydrocarbons). In the present study, most of the high-
558 intensity CHON, CHO, and CHN compounds with high AI values were clustered in
559 potential BrC chromophore region (Figures S3 and S4), which mainly comprised CHON
560 (46%–50% in ESI⁻ mode and 56%–62% in ESI⁺ mode, respectively) and CHO (44%–48%
561 in ESI⁻ mode and 29%–38% in ESI⁺ mode, respectively) compounds (Table 1).
562 Although the contribution of CHN⁺ compounds to BrC was relatively lower, the content
563 of potential chromophores among the total CHN⁺ compounds was higher than those in

564 CHON⁺ and CHO⁺ compounds. Therefore, these three groups of light-absorbing
565 compounds (i.e., CHON⁺, CHN⁺, and CHO⁺ compounds) were further examined. As
566 shown in Table 1, the Int_C/Int_{BrC} values of CHO⁻ (i.e., content of CHO⁻ chromophores
567 in the total chromophores) decreased from 48% to 44% whereas the Int_C/Int_{BrC} values of
568 CHON⁻ increased from 46% to 50% during the haze bloom process. These findings
569 indicated that more NOCs chromophores were formed during this stage in which higher
570 NO₂ concentration may be preferred for the formation of N-containing chromophores
571 such as nitrophenols. However, it must be noted that the proportions of both CHO⁻ and
572 CHON⁻ chromophores among the total identified compounds decreased from clean-I to
573 haze-I days, suggesting the occurrence of stronger photo-bleaching process during the
574 haze bloom stage (Zeng et al., 2020). Likewise, both CHO⁺ and CHON⁺ compounds
575 presented similar variation during the entire study period. In addition, the CHN⁺
576 compounds also exhibited higher Int_C/Int_{BrC} values during the haze bloom process and
577 suggesting the accumulated contribution from local combustion process. Furthermore, the
578 proportion of CHON⁺ chromophores in the total CHON⁺ compounds increased with the
579 decreasing content of CHN⁺ chromophores, may implying that some aromatic CHN⁺
580 compounds were transformed to CHON⁺ compounds during the aging process.

581

582 **4. Conclusions**

583 This study investigated the evolution of light absorption and molecular properties of
584 HULIS during a winter haze bloom-decay process, and examined the key factors
585 affecting the light absorption of HULIS in Guangzhou, China. The results showed that
586 HULIS exhibited significant variation in light absorption during the haze bloom-decay

587 process. First, higher Abs₃₆₅ values were observed in haze days, indicating the presence
588 of significant amounts of light-absorbing organic compounds during the haze episode.
589 However, the MAE₃₆₅ values for HULIS in haze days were relatively lower than those in
590 clean days, suggesting the light absorption capabilities of HULIS were weakened during
591 the haze event. Furthermore, CHON and CHO compounds, exhibiting relatively higher
592 degree of conjugated structure, were the most abundant groups in all the HULIS samples,
593 and were also the major contributors to light absorption capacity of HULIS. Importantly,
594 the molecular properties of HULIS dynamically varied during the entire haze episode.
595 When compared with HULIS in clean days, those in haze days presented relatively lower
596 AI_{mod} values and higher O/C_w, O/N_w, and O/S_w ratios, suggesting the predominance of
597 compounds with low aromaticity and higher oxidation in HULIS during haze episode.
598 These results indicated that HULIS compounds undergo relatively stronger oxidation
599 during the haze days. Moreover, PCA and Pearson correlation analysis revealed that BB
600 and secondary chemical formation both contributed to the variation in the light absorption
601 properties of HULIS. Both primary sources (such as accumulated contribution of organic
602 compounds formed from local traffic emission) and secondary sources (such as stronger
603 chemical reactions) led to the rapid increase in HULIS during the haze bloom days.
604 However, stronger oxidation of HULIS compounds were observed during the haze
605 episode, and some potential BrC chromophores were degraded. In addition, the chemical
606 reactions of bio-VOCs such as isoprene also diluted the light-absorbing compounds in
607 HULIS.

608 Thus, the present study provides novel insights into the light and molecular
609 evolution of HULIS during haze event, which are important for predicting the

610 environmental and climatic effects of HULIS. However, as this study examined only one
611 haze bloom-decay process in winter in Guangzhou, the results obtained may be not
612 adequate for understanding all the haze episodes in South China. Therefore, there is a
613 need for a comprehensive investigation of haze episode in different seasons and regions
614 in future.

615

616 **Data availability**

617 The research data are available in the Harvard Dataverse
618 (<https://doi.org/10.7910/DVN/DYGYQT>, Song, 2022).

619

620 **Author contributions.** J. Song and P. Peng designed the research together. C, Zou, T.
621 Cao, and M. Li carried out the PM_{2.5} sampling experiments. C, Zou and T. Cao extracted
622 and analyzed the WSOC and HULIS samples. B. Jiang analyzed the HULIS samples by
623 FT-ICR MS. C. Zou and J. Song wrote the paper. J. Li, X. Ding, Z Yu, and G. Zhang
624 commented and revised the paper.

625

626 **Competing interests.** The authors declare that they have no conflict of interest

627

628 **Acknowledgments.** This study was supported by the National Natural Science
629 Foundation of China (42192514 and 41977188), Guangdong Foundation for Program of
630 Science and Technology Research (2020B1212060053), and Guangdong Foundation for
631 Program of Science and Technology Research (2019B121205006).

632

633 **References**

634 An, Z., Huang, R. J., Zhang, R., Tie, X., Li, G., Cao, J., Zhou, W., Shi, Z., Han, Y., Gu,
635 Z., and Ji, Y.: Severe haze in northern China: A synergy of anthropogenic emissions
636 and atmospheric processes, *Proc Natl Acad Sci USA*, 116, 8657-8666,
637 10.1073/pnas.1900125116, 2019.

638 Berkemeier, T., Ammann, M., Mentel, T. F., Poschl, U., and Shiraiwa, M.: Organic
639 nitrate contribution to new particle formation and growth in secondary organic
640 aerosols from alpha-pinene ozonolysis, *Environ Sci Technol*, 50, 6334-6342,
641 10.1021/acs.est.6b00961, 2016.

642 Bianco, A., Deguillaume, L., Vaitilingom, M., Nicol, E., Baray, J. L., Chaumerliac, N.,
643 and Bridoux, M.: Molecular characterization of cloud water samples collected at the
644 Puy de Dome (France) by Fourier transform ion cyclotron resonance mass
645 spectrometry, *Environ Sci Technol*, 52, 10275-10285, doi:10.1021/acs.est.8b01964,
646 2018.

647 Cao, T., Li, M., Zou, C., Fan, X., Song, J., Jia, W., Yu, C., Yu, Z., Peng, P.: Chemical
648 composition, optical properties, and oxidative potential of water-and methanol-
649 soluble organic compounds emitted from the combustion of biomass materials and
650 coal, *Atmos Chem Phys*, 21, 13187-13205, doi: 10.5194/acp-21-13187-2021, 2021.

651 Chen, Q., Ikemori, F., Mochida, M.: Light absorption and excitation-emission
652 fluorescence of urban organic aerosol components and their relationship to chemical
653 structure, *Environ. Sci. Technol.*, 50, 10859-10868, doi: 10.1021/acs.est.6b02541,
654 2016.

655 Cui, M., Li, C., Chen, Y. J., Zhang, F., Li, J., Jiang, B., Mo, Y., Li, J., Yan, C., Zheng,
656 M., Xie, Z., Zhang, G., and Zheng, J.: Molecular characterization of polar organic
657 aerosol constituents in off-road engine emissions using Fourier transform ion
658 cyclotron resonance mass spectrometry (FT-ICR MS): implications for source
659 apportionment, *Atmos Chem Phys*, 19, 13945-13956, doi:10.5194/acp-19-13945-
660 2019, 2019.

661 Dasari, S., Andersson, A., Bikkina, S., Holmstrand, H., Budhavant, K., Satheesh, S.,
662 Asmi, E., Kesti, J., Backman, J., Salam, A., Bisht, D. S., Tiwari, S., Hameed, Z., and
663 Gustafsson, Ö.: Photochemical degradation affects the light absorption of water-
664 soluble brown carbon in the South Asian outflow, *Sci Adv*, 5, eaau8066, doi:
665 10.1126/sciadv.aau8066, 2019.

666 Decesari, S., Facchini, M. C., Matta, E., Mircea, M., Fuzzi, S., Chughtai, A. R., and
667 Smith, D. M.: Water soluble organic compounds formed by oxidation of soot, *Atmos*
668 *Environ*, 36, 1827-1832, 10.1016/s1352-2310(02)00141-3, 2002.

669 Deng, J., Ma, H., Wang, X., Zhong, S., Zhang, Z., Zhu, J., Fan, Y., Hu, W., Wu, L., Li,
670 X., Ren, L., Pavuluri, C.M., Pan, X., Sun, Y., Wang, Z., Kawamura, K., and Fu, P.:
671 Measurement report: Optical properties and sources of water-soluble brown carbon
672 in Tianjin, North China –insights from organic molecular compositions, *Atmos.*
673 *Chem. Phys.*, 22, 6449–6470, doi: 10.5194/acp-22-6449-2022, 2022.

674 Du, Z., He, K., Cheng, Y., Duan, F., Ma, Y., Liu, J., Zhang, X., Zheng, M., and Weber,
675 R.: A yearlong study of water-soluble organic carbon in Beijing II: Light absorption
676 properties, *Atmos Environ*, 89, 235-241, 10.1016/j.atmosenv.2014.02.022, 2014.

677 Fan, X. J., Song, J. Z., and Peng, P. A.: Comparison of isolation and quantification
678 methods to measure humic-like substances (HULIS) in atmospheric particles, *Atmos.*
679 *Environ.*, 60, 366–374, 10.1016/j.atmosenv.2012.06.063, 2012.

680 Fan, X., Song, J., Peng, P.: Comparative study for separation of atmospheric humiclike
681 substance (HULIS) by ENVI-18, HLB, XAD-8 and DEAE sorbents: elemental
682 composition, FT-IR, ¹H-NMR and off-line thermochemolysis with
683 tetramethylammonium hydroxide (TMAH). *Chemosphere* 93, 1710–1719,
684 10.1016/j.chemosphere.2013.05.045, 2013.

685 Fan, X., Song, J., and Peng, P.: Temporal variations of the abundance and optical
686 properties of water soluble Humic-Like Substances (HULIS) in PM_{2.5} at Guangzhou,
687 China, *Atmos Res*, 172-173, 8-15, doi:10.1016/j.atmosres.2015.12.024, 2016.

688 Fan, X., Cao, T., Yu, X., Wang, Y., Xiao, X., Li, F., Xie, Y., Ji, W., Song, J., and Peng, P:
689 The evolutionary behavior of chromophoric brown carbon during ozone aging of fine
690 particles from biomass burning, *Atmos Chem Phys*, 20, 4593-4605, doi:10.5194/acp-
691 20-4593-2020, 2020.

692 Forrister, H., Liu, J., Scheuer, E., Dibb, J., Ziemba, L., Thornhill, K. L., Anderson, B.,
693 Diskin, G., Perring, A. E., Schwarz, P., Campuzano-Jost, P., Day, D. A., Palm, B. B.,
694 Jimenez, J. L., Nenes, A., and Weber, R. J.: Evolution of brown carbon in wildfire
695 plumes, *Geophys. Res. Lett.*, 42, 4623–4630, doi: 10.1002/2015gl063897, 2015.

696 Graber and Rudich: Atmospheric HULIS: How humic-like are they? A comprehensive
697 and critical review, *Atmos Chem Phys*, 6, 729-753, 2006.

698 Huang, R. J., Yang, L., Cao, J., Chen, Y., Chen, Q., Chen, Q., Li, Y. J., Duan, J., Zhu, C.
699 C., Dai, W. T., Wang, K., Lin, C. S., Ni, H. Y., Corbin, J. C., Wu, Y. F., Zhang, R. J.

700 Tie, X. X., Hoffmann, T., O'Dowd, C., and Dusek, U.: Brown carbon aerosol in
701 urban Xi'an, Northwest China: The composition and light absorption properties,
702 *Environ Sci Technol*, 52, 6825-6833, doi:10.1021/acs.est.8b02386, 2018.

703 Huang, R. J., Yang, L., Shen, J. C., Yuan, W., Gong, Y. Q., Guo, J., Cao, W., Duan, J.,
704 Ni, H., Zhu, C., Dai, W., Li, Y., Chen, Y., Chen, Q., Wu, Y., Zhang, R., Dusek, U.,
705 O'Dowd, C., and Hoffmann, T.: Water-insoluble organics dominate brown carbon in
706 wintertime urban aerosol of China: chemical characteristics and optical properties,
707 *Environ Sci Technol*, 54, 7836-7847, doi:10.1021/acs.est.0c01149, 2020.

708 Jiang, B., Kuang, B. Y., Liang, Y., Zhang, J., Huang, X. H. H., Xu, C., Yu, J. Z., and Shi,
709 Q.: Molecular composition of urban organic aerosols on clear and hazy days in
710 Beijing: a comparative study using FT-ICR MS, *Environ. Chem.*, 13, 888–901,
711 <https://doi.org/10.1071/en15230>, 2016.

712 Jiang, H., Li, J., Chen, D., Tang, J., Cheng, Z., Mo, Y., Su, T., Tian, C., Jiang, B., Liao,
713 Y., and Zhang, G.: Biomass burning organic aerosols significantly influence the light
714 absorption properties of polarity-dependent organic compounds in the Pearl River
715 Delta Region, China, *Environ Int*, 144, 106079, 10.1016/j.envint.2020.106079, 2020.

716 Jiang, H., Li, J., Sun, R., Liu, G., Tian, C., et al. Determining the sources and transport
717 of brown carbon using radionuclide tracers and modeling, *J Geophys Res Atmos*,
718 126, e2021JD034616, doi:org/10.1029/2021JD034616, 2021.

719 Kampf, C. J., Filippi, A., Zuth, C., Hoffmann, T., and Opatz, T.: Secondary brown
720 carbon formation via the dicarbonyl imine pathway: nitrogen heterocycle formation
721 and synergistic effects, *Phys Chem Chem Phys*, 18, 18353-18364,
722 10.1039/c6cp03029g, 2016.

723 Kroll, J. H., Donahue, N. M., Jimenez, J. L., Kessler, S. H., Canagaratna, M. R., Wilson,
724 K. R., Altieri, K. E., Mazzoleni, L. R., Wozniak, A. S., Bluhm, H., Mysak, E. R.,
725 Smith, J. D., Kolb, C. E., and Worsnop, D. R.: Carbon oxidation state as a metric for
726 describing the chemistry of atmospheric organic aerosol, *Nature Chem*, 3, 133-139,
727 10.1038/nchem.948, 2011.

728 Kuang, K. and Shang, J.: Changes in light absorption by brown carbon in soot particles
729 due to heterogeneous ozone aging in a smog chamber, *Environ Pollut*, 266, 115273,
730 10.1016/j.envpol.2020.115273, 2020.

731 Laskin, A., Laskin, J., and Nizkorodov, S. A.: Chemistry of atmospheric brown carbon,
732 *Chem Rev*, 115, 4335-4382, 10.1021/cr5006167, 2015.

733 Li, K., Jacob, D. J., Liao, H., Shen, L., Zhang, Q., and Bates, K.H.: Anthropogenic
734 drivers of 2013–2017 trends in summer surface ozone in China, *Proc Natl Acad Sci*
735 *USA*, 116, 422–427, <https://doi.org/10.1073/pnas.1812168116>, 2019.

736 Li, M., Fan, X., Zhu, M., Zou, C., Song, J., Wei, S., Jia, W., and Peng, P.: Abundance
737 and light absorption properties of brown carbon emitted from residential coal
738 combustion in China, *Environ Sci Technol*, 53, 595-603,
739 doi:10.1021/acs.est.8b05630, 2019.

740 Li, S. W., Chang, M., Li, H., Cui, X. Y., and Ma, L. Q.: Chemical compositions and
741 source apportionment of PM_{2.5} during clear and hazy days: seasonal changes and
742 impacts of Youth Olympic Games, *Chemosphere*, 256, 127163,
743 10.1016/j.chemosphere.2020.127163, 2020.

744 Li, P. and Hur, J., Utilization of UV-Vis spectroscopy and related data analyses for
745 dissolved organic matter (DOM) studies: A review, *Crit. Rev. Environ. Sci. Technol.*,
746 47, 131–154, doi: 10.1080/10643389.2017.1309186, 2017.

747 Lin, P.; Engling, G.; Yu, J. Z.: Humic-like substances in fresh emissions of rice straw
748 burning and in ambient aerosols in the Pearl River Delta Region, China. *Atmos*
749 *Chem Phys*, 10, 6487–6500, 10.5194/acp-10-6487-2010, 2010.

750 Lin, P., Bluvshstein, N., Rudich, Y., Nizkorodov, S. A., Laskin, J., and Laskin, A.:
751 Molecular chemistry of atmospheric brown carbon inferred from a nationwide
752 biomass burning event, *Environ Sci Technol*, 51, 11561-11570,
753 10.1021/acs.est.7b02276, 2017.

754 Lin, P., Rincon, A. G., Kalberer, M., and Yu, J. Z.: Elemental composition of HULIS in
755 the Pearl River Delta Region, China: results inferred from positive and negative
756 electrospray high resolution mass spectrometric data, *Environ Sci Technol*, 46, 7454-
757 7462, 10.1021/es300285d, 2012.

758 Lin, P., Fleming, L. T., Nizkorodov, S. A., Laskin, J., and Laskin, A.: Comprehensive
759 molecular characterization of atmospheric brown carbon by high resolution mass
760 spectrometry with electrospray and atmospheric pressure photoionization, *Anal*
761 *Chem*, 90, 12493-12502. doi:10.1021/acs.analchem.8b02177, 2018.

762 Liu, J., Lin, P., Laskin, A., Laskin, J., Kathmann, S. M., Wise, M., Caylor, R., Imholt, F.,
763 Selimovic, V., and Shilling, J. E.: Optical properties and aging of light-absorbing
764 secondary organic aerosol, *Atmos Chem Phys*, 16, 12815-12827, 10.5194/acp-16-
765 12815-2016, 2016.

766 Liu, J., Mo, Y., Ding, P., Li, J., Shen, C., and Zhang, G.: Dual carbon isotopes (^{14}C
767 and ^{13}C) and optical properties of WSOC and HULIS-C during winter in
768 Guangzhou, China, *Sci Total Environ*, 633, 1571-1578,
769 10.1016/j.scitotenv.2018.03.293, 2018.

770 Ma, Y., Cheng, Y., Qiu, X., Cao, G., Kuang, B., Yu, J. Z., and Hu, D.: Optical properties,
771 source apportionment and redox activity of humic-like substances (HULIS) in
772 airborne fine particulates in Hong Kong, *Environ Pollut*, 255, 113087,
773 10.1016/j.envpol.2019.113087, 2019.

774 Mo, Y., Li, J., Jiang, B., Su, T., Geng, X., Liu, J., Jiang, H., Shen, C., Ding, P., Zhong, G.,
775 Cheng, Z., Liao, Y., Tian, C., Chen, Y., and Zhang, G.: Sources, compositions, and
776 optical properties of humic-like substances in Beijing during the 2014 APEC summit:
777 Results from dual carbon isotope and Fourier-transform ion cyclotron resonance
778 mass spectrometry analyses, *Environ Pollut*, 239, 322-331,
779 10.1016/j.envpol.2018.04.041, 2018.

780 Mohr, C., Lopez-Hilfiker, F. D., Zotter, P., Prevot, A. S., Xu, L., Ng, N. L., Herndon, S.
781 C., Williams, L. R., Franklin, J. P., Zahniser, M. S., Worsnop, D. R., Knighton, W.
782 B., Aiken, A. C., Gorkowski, K. J., Dubey, M. K., Allan, J. D., and Thornton, J. A.:
783 Contribution of nitrated phenols to wood burning brown carbon light absorption in
784 Detling, United Kingdom during winter time, *Environ Sci Technol*, 47, 6316-6324,
785 10.1021/es400683v, 2013.

786 Ni, H., Huang, R. J., Pieber, S. M., Corbin, J. C., Stefenelli, G., Pospisilova, V., Klein, F.,
787 Gysel-Beer, M., Yang, L., Baltensperger, U., Haddad, I. E., Slowik, J. G., Cao, J.,

788 Prevot, A. S. H., and Dusek, U.: Brown carbon in primary and aged coal combustion
789 emission, *Environ Sci Technol*, 55, 5701-5710, 10.1021/acs.est.0c08084, 2021.

790 Park, S., Yua, G.-H., and Lee, S., Optical absorption characteristics of brown carbon
791 aerosols during the KORUS-AQ campaign at an urban site, *Atmos. Res.*, 203, 16–27,
792 doi: 10.1016/j.atmosres.2017.12.002, 2018.

793 Saleh, R., Hennigan, C. J., McMeeking, G. R., Chuang, W. K., Robinson, E. S., Coe, H.,
794 Donahue, N. M., and Robinson, A. L.: Absorptivity of brown carbon in fresh and
795 photo-chemically aged biomass-burning emissions, *Atmos. Chem. Phys.*, 13, 7683–
796 7693, doi: 10.5194/acp-13-7683-2013, 2013.

797 Shen, Z., Zhang, Q., Cao, J., Zhang, L., Lei, Y., Huang, Y., Huang, R. J., Gao, J., Zhao,
798 Z., Zhu, C., Yin, X., Zheng, C., Xu, H., and Liu, S.: Optical properties and possible
799 sources of brown carbon in PM 2.5 over Xi'an, China, *Atmos Environ*, 150, 322-330,
800 10.1016/j.atmosenv.2016.11.024, 2017.

801 Song, J.: Data for SJ, Harvard Dataverse [data set],
802 (<https://doi.org/10.7910/DVN/DYGYQT>), 2022.

803 Song, J. Z., Li, M. J., Fan, X. J., Zou, C. L., Zhu, M. B., Jiang, B., Yu, Z. Q., Jia, W. L.,
804 Liao, Y. H., and Peng, P. A.: Molecular characterization of water- and methanol-
805 soluble organic compounds emitted from residential coal combustion using
806 ultrahigh-resolution electrospray ionization Fourier transform ion cyclotron
807 resonance mass spectrometry, *Environ Sci Technol*, 53, 13607-13617,
808 10.1021/acs.est.9b04331, 2019.

809 Song, J. Z., Li, M. J., Jiang, B., Wei, S. Y., Fan, X. J., and Peng, P. A.: Molecular
810 Characterization of Water-Soluble Humic like substances in smoke particles emitted

811 from combustion of biomass materials and coal using ultrahigh-resolution
812 electrospray ionization Fourier transform ion cyclotron resonance mass spectrometry,
813 *Environ Sci Technol*, 52, 2575-2585, 10.1021/acs.est.7b06126, 2018.

814 Song, J. Z., Li, M. J., Zou, C. L., Cao, T., Fan, X. J., Jiang, B., Yu, Z. Q., Jia, W. L., and
815 Peng, P. A.: Molecular characterization of nitrogen-containing compounds in humic-
816 like substances emitted from biomass burning and coal combustion, *Environ Sci*
817 *Technol*, 56, 119-130, doi:10.1021/acs.est.1c04451, 2022.

818 Sumlin, B. J., Pandey, A., Walker, M. J., Pattison, R. S., Williams, B. J., and Chakrabarty,
819 R. K.: Atmospheric photooxidation diminishes light absorption by primary brown
820 carbon aerosol from biomass burning, *Environ Sci Tech Lett*, 4, 540-545,
821 10.1021/acs.estlett.7b00393, 2017.

822 Surratt, J. D., Gomez-Gonzalez, Y., Chan, A. W. H., Vermeylen, R., Shahgholi, M.,
823 Kleindienst, T. E., Edney, E. O., Offenberg, J. H., Lewandowski, M., Jaoui, M.,
824 Maenhaut, W., Claeys, M., Flagan, R. C., and Seinfeld, J. H.: Organosulfate
825 formation in biogenic secondary organic aerosol, *J Phys Chem A*, 112, 8345-8378,
826 10.1021/jp802310p, 2008.

827 Tan, J., Xiang, P., Zhou, X., Duan, J., Ma, Y., He, K., Cheng, Y., Yu, J., and Querol, X.:
828 Chemical characterization of humic-like substances (HULIS) in PM_{2.5} in Lanzhou,
829 China, *Sci Total Environ*, 573, 1481-1490, 10.1016/j.scitotenv.2016.08.025, 2016.

830 Tang, J., Li, J., Su, T., Han, Y., Mo, Y. Z., Jiang, H. X., Cui, M., Jiang, B., Chen, Y. J.,
831 Tang, J. H., Song, J. Z., Peng, P. A., and Zhang, G.: Molecular compositions and
832 optical properties of dissolved brown carbon in biomass burning, coal combustion,
833 and vehicle emission aerosols illuminated by excitation-emission matrix

834 spectroscopy and Fourier transform ion cyclotron resonance mass spectrometry
835 analysis, *Atmos Chem Phys*, 20, 2513-2532, 10.5194/acp-20-2513-2020, 2020.

836 Tomaz, S., Cui, T., Chen, Y., Sexton, K. G., Roberts, J. M., Warneke, C., Yokelson, R. J.,
837 Surratt, J. D., and Turpin, B. J.: Photochemical Cloud Processing of primary wildfire
838 emissions as a potential source of secondary organic Aerosol, *Environ Sci Technol*, 52,
839 11027-11037, 10.1021/acs.est.8b03293, 2018.

840 Wang, J., Wang, G., Gao, J., Wang, H., Ren, Y., Li, J., Zhou, B., Wu, C., Zhang, L.,
841 Wang, S., and Chai, F.: Concentrations and stable carbon isotope compositions of
842 oxalic acid and related SOA in Beijing before, during, and after the 2014 APEC,
843 *Atmos Chem Phys*, 17, 981-992, 10.5194/acp-17-981-2017, 2017a.

844 Wang, X. K., Hayeck, N., Brüggemann, M., Yao, L., Chen, H. F., Zhang, C., Emmelin,
845 C., Chen, J. M., George, C., and Wang, L.: Chemical characteristics of organic
846 aerosols in shanghai: a study by ultrahigh-performance liquid chromatography
847 coupled with orbitrap mass spectrometry, *J Geophys Res Atmos*, 122, 11703-11722,
848 10.1002/2017jd026930, 2017b.

849 Wang, Y., Hu, M., Lin, P., Tan, T., Li, M., Xu, N., Zheng, J., Du, Z., Qin, Y., Wu, Y., Lu,
850 S., Song, Y., Wu, Z., Guo, S., Zeng, L., Huang, X., and He, L.: Enhancement in
851 particulate organic nitrogen and light absorption of humic-like substances over
852 Tibetan Plateau due to long-range transported biomass burning emissions, *Environ*
853 *Sci Technol*, 53, 14222-14232, 10.1021/acs.est.9b06152, 2019.

854 Wang, X., Hayeck, N., Brüggemann, M., Abis, L., Riva, M., Lu, Y., Wang, B., Chen, J.,
855 George, C., and Wang, L.: Chemical characteristics and brown carbon chromophores

856 of atmospheric organic aerosols over the Yangtze River channel: a cruise campaign,
857 J Geophys Res Atmos, 125, 10.1029/2020jd032497, 2020.

858 Wong, J. P. S., Nenes, A., and Weber, R. J.: Changes in Light Absorptivity of Molecular
859 Weight Separated Brown Carbon Due to Photolytic Aging, Environ Sci Technol, 51,
860 8414-8421, 10.1021/acs.est.7b01739, 2017.

861 Wu, Z., Wang, Y., Tan, T., Zhu, Y., Li, M., Shang, D., Wang, H., Lu, K., Guo, S., Zeng,
862 L., and Zhang, Y.: Aerosol liquid water driven by anthropogenic inorganic salts:
863 implying its key role in haze formation over the North China Plain, Environ Sci
864 Technol Lett, 5, 160-166, 10.1021/acs.estlett.8b00021, 2018.

865 Yang, X., Lu, K., Ma, X., Gao, Y., Tan, Z., Wang, H., Chen, X., Li, X., Huang, X., He,
866 L., Tang, M., Zhu, B., Chen, S., Dong, H., Zeng, L., and Zhang, Y.: Radical
867 chemistry in the Pearl River Delta: observations and modeling of OH and HO₂
868 radicals in Shenzhen in 2018. Atmos Chem Phys, 22, 12525-12542, 10.5194/acp-22-
869 12525-2022, 2022.

870 Yu, L., Smith, J., Laskin, A., George, K. M., Anastasio, C., Laskin, J., Dillner, A. M.,
871 and Zhang, Q.: Molecular transformations of phenolic SOA during photochemical
872 aging in the aqueous phase: competition among oligomerization, functionalization,
873 and fragmentation, Atmos Chem Phys, 16, 4511-4527, 10.5194/acp-16-4511-2016,
874 2016.

875 Yu, X., Yu, Q., Zhu, M., Tang, M., Li, S., Yang, W., Zhang, Y., Deng, W., Li, G., Yu, Y.,
876 Huang, Z., Song, W., Ding, X., Hu, Q., Li, J., Bi, X., and Wang, X.: Water soluble
877 organic nitrogen (WSON) in ambient fine particles over a megacity in South China:

878 spatiotemporal variations and source apportionment, *J Geophys Res Atmos*, 122,
879 10.1002/2017jd027327, 2017.

880 Yuan, W., Huang, R. J., Yang, L., Ni, H., Wang, T., Cao, W., Duan, J., Guo, J., Huang,
881 H., and Hoffmann, T.: Concentrations, optical properties and sources of humic-like
882 substances (HULIS) in fine particulate matter in Xi'an, Northwest China, *Sci Total*
883 *Environ*, 789, 147902, 10.1016/j.scitotenv.2021.147902, 2021.

884 Zeng, Y., Shen, Z., Takahama, S., Zhang, L., Zhang, T., Lei, Y., Zhang, Q., Xu, H., Ning,
885 Y., Huang, Y., Cao, J., and Rudolf, H.: Molecular Absorption and Evolution
886 Mechanisms of PM 2.5 Brown carbon revealed by electrospray ionization Fourier
887 transform-ion cyclotron resonance mass spectrometry during a severe winter
888 pollution episode in Xi'an, China, *Geophys Res Lett*, 47, 10.1029/2020gl087977,
889 2020.

890 Zhan, Y., Li, J., Tsona, N.T., Chen, B., Yan, C., George, C., and Du, L.: Seasonal
891 variation of water-soluble brown carbon in Qingdao, China: Impacts from marine
892 and terrestrial emissions, *Environ. Res.*, 212, 113144, doi:
893 10.1016/j.envres.2022.113144, 2022.

894 Zhang, J., Liu, L., Xu, L., Lin, Q., Zhao, H., Wang, Z., Guo, S., Hu, M., Liu, D., Shi, Z.,
895 Huang, D., and Li, W.: Exploring wintertime regional haze in northeast China: role of
896 coal and biomass burning, *Atmos Chem Phys*, 20, 5355-5372, 10.5194/acp-20-5355-
897 2020, 2020.

898 Zhang, L., Wang, G., Wang, J., Wu, C., Cao, C., and Li, J.: Chemical composition of
899 fine particulate matter and optical properties of brown carbon before and during
900 heating season in Xi'an, *Journal of Earth Environment*, 8, 451-458, 2017.

901 Zhang, Q., Worsnop, D. R., Canagaratna, M. R., and Jimenez, J. L.: Hydrocarbon-like
902 and oxygenated organic aerosols in Pittsburgh: insights into sources and processes of
903 organic aerosols, *Atmos Chem Phys*, 5, 3289-3311, 10.5194/acp-5-3289-2005, 2005.

904 Zhang, Y.-L., El-Haddad, I., Huang, R.-J., Ho, K.-F., Cao, J.-J., Han, Y., Zotter, P.,
905 Bozzetti, C., Daellenbach, K. R., Slowik, J. G., Salazar, G., Prévôt, A. S. H., and
906 Szidat, S.: Large contribution of fossil fuel derived secondary organic carbon to water
907 soluble organic aerosols in winter haze in China, *Atmos Chem Phys*, 18, 4005-4017,
908 10.5194/acp-18-4005-2018, 2018.

909 Zhong, M. and Jang, M.: Dynamic light absorption of biomass-burning organic carbon
910 photochemically aged under natural sunlight, *Atmos Chem Phys*, 14, 1517-1525,
911 10.5194/acp-14-1517-2014, 2014.

912 Zhu, C. S., Cao, J. J., Huang, R. J., Shen, Z. X., Wang, Q. Y., and Zhang, N. N.: Light
913 absorption properties of brown carbon over the southeastern Tibetan Plateau, *Sci*
914 *Total Environ*, 625, 246-251, 10.1016/j.scitotenv.2017.12.183, 2018.

915 Zou, C., Li, M., Cao, T., Zhu, M., Fan, X., Peng, S., Song, J., Jiang, B., Jia, W., Yu, C.,
916 Song, H., Yu, Z., Li, J., Zhang, G., and Peng, P. a.: Comparison of solid phase
917 extraction methods for the measurement of humic-like substances (HULIS) in
918 atmospheric particles, *Atmos Environ*, 225, 117370,
919 10.1016/j.atmosenv.2020.117370, 2020.

920

921

922
 923
 924
 925
 926
 927
 928
 929
 930
 931
 932
 933
 934
 935
 936
 937
 938
 939
 940
 941
 942
 943
 944
 945
 946
 947
 948
 949
 950
 951
 952

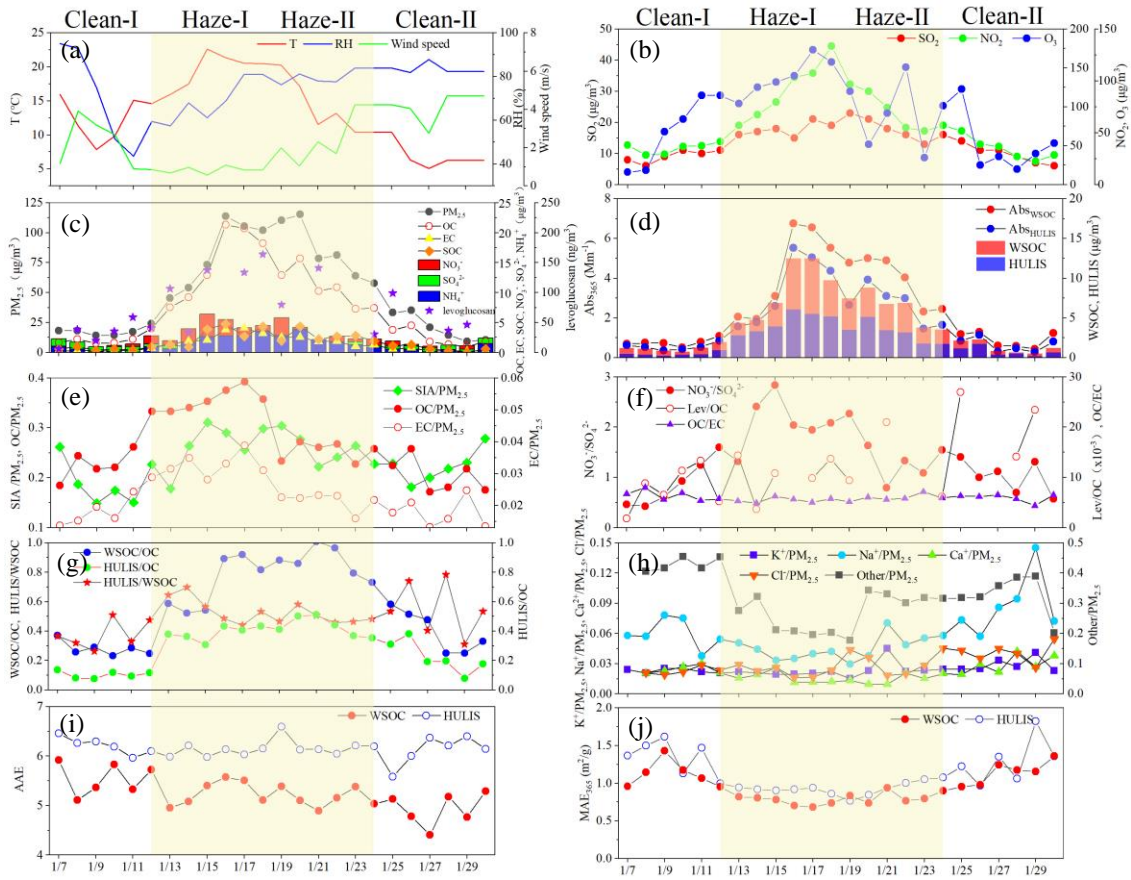


Figure 1. Temporal variation in meteorological parameters, concentrations of chemical composition, and optical properties (Abs_{365} , MAE_{365} , and AAE) of water-soluble BrC in the $PM_{2.5}$ samples.

953

954

955

956

957

958

959

960

961

962

963

964

965

966

967

968

969

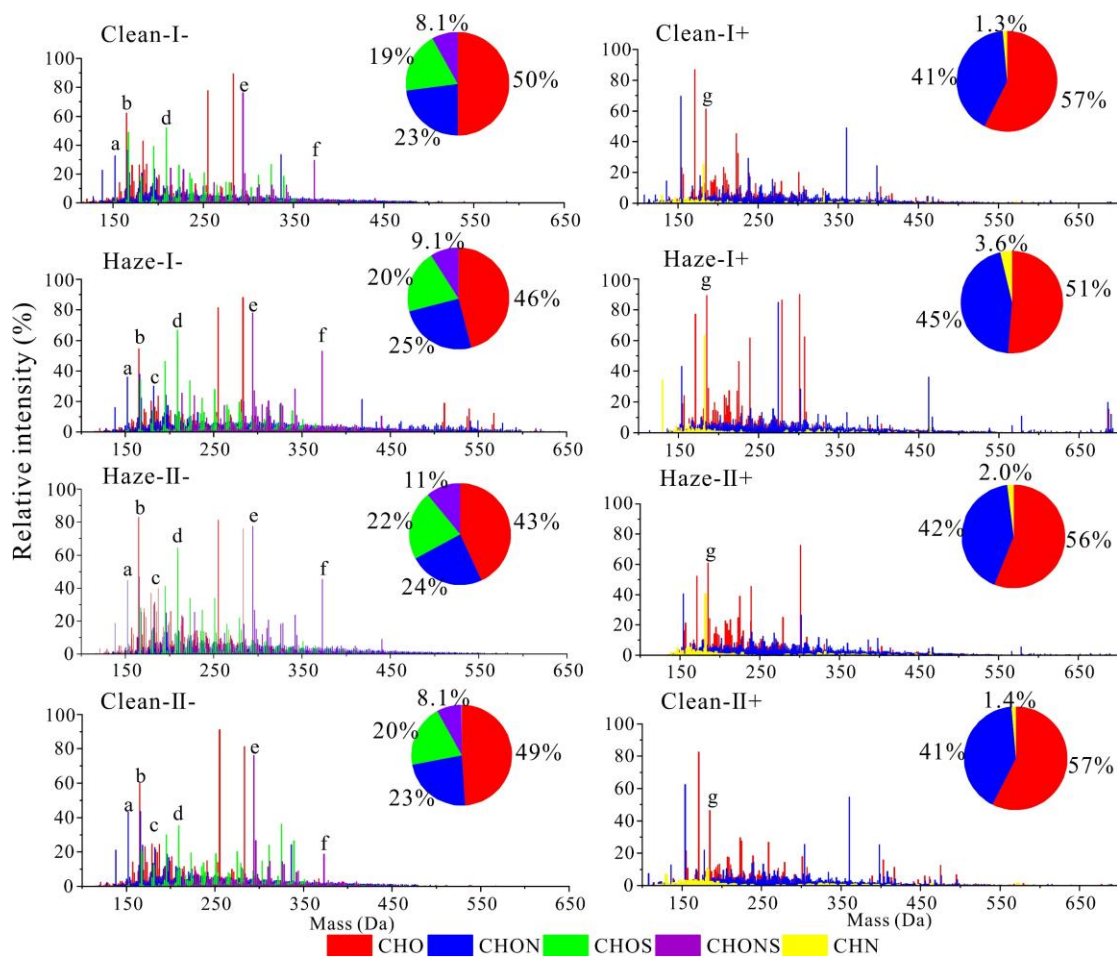
970

971

972

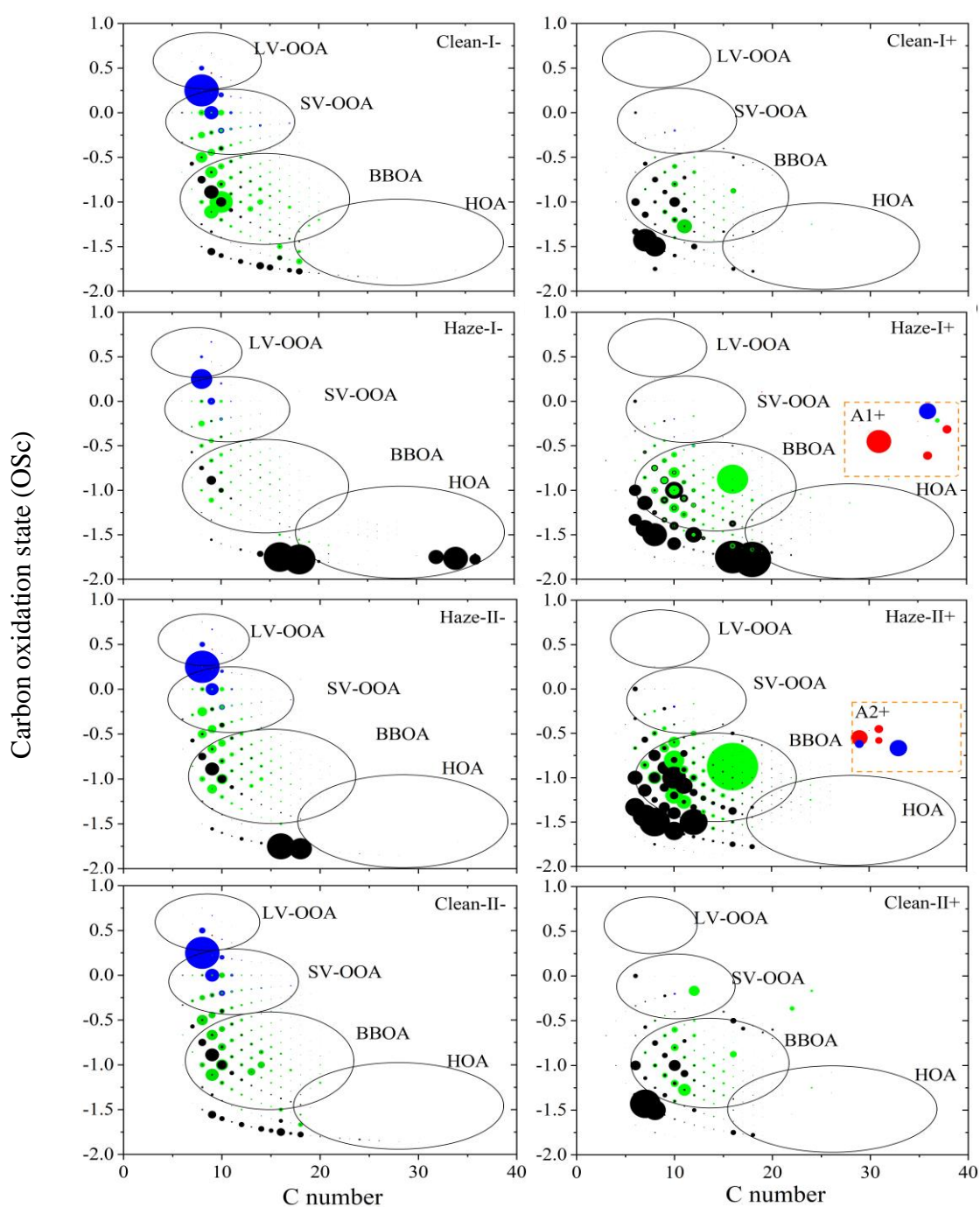
973

974



975 **Figure 2.** Mass spectra of HULIS detected in ESI- and ESI+ modes during the
976 haze process. The pie charts represent the intensity percent of different compound groups.
977

978



1010 **Figure 3.** Carbon oxidation state (OSc) plots for CHO- and CHO+. Formulas with black,
 1011 green, blue, and red are assigned to aliphatic (AI = 0), olefinic ($0 < AI < 0.5$), aromatic
 1012 ($0.5 \leq AI < 0.67$), and condensed aromatic ($AI \geq 0.67$) species (Koch and Dittmar, 2006),
 1013 respectively.

1014

1015

1016

1017

1018

1019

1020

1021

1022

1023

1024

1025

1026

1027

1028

1029

1030

1031

1032

1033

1034

1035

1036

1037

1038

1039

1040

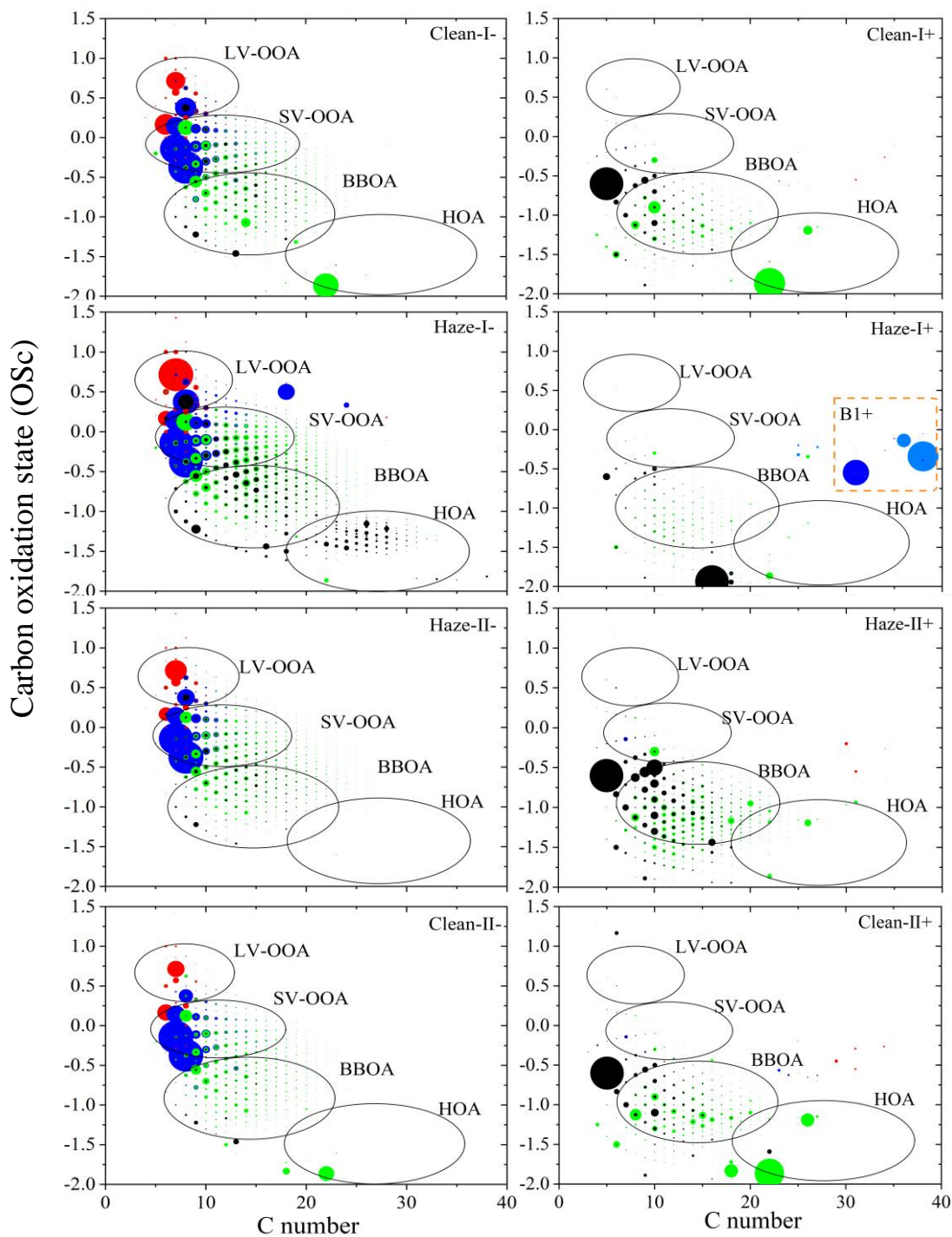
1041

1042

1043

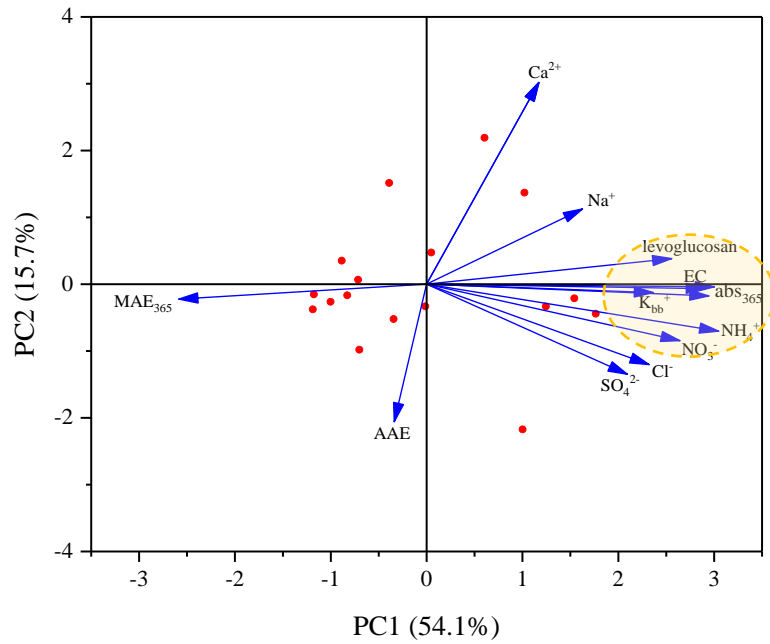
1044

1045



1046 **Figure 4.** Carbon oxidation state (OSc) plots for CHON- and CHON+. Formulas with
1047 black, green, blue, and red are assigned to aliphatic ($AI = 0$), olefinic ($0 < AI < 0.5$),
1048 aromatic ($0.5 \leq AI < 0.67$), and condensed aromatic ($AI \geq 0.67$) species (Koch and Dittmar,
1049 2006), respective.

1050
1051
1052
1053
1054
1055
1056
1057
1058
1059
1060
1061
1062
1063
1064
1065
1066



1067 **Figure 5.** Principal component analysis results for the optical properties of HULIS and
1068 chemical compositions of PM_{2.5}.
1069